REFERENCES

[1] L. Sentis, "Synthesis and control of whole-body behaviors in humanoid systems," Ph.D. dissertation, Stanford Univ., Stanford, CA, 2007.

[2] K. F. Zabjek, C. Coillard, C. H. Rivard, and F. Prince, "Estimation of the center of mass for the study of postural control in idiopathic scoliosis patients: A comparison of two techniques," *Eur. Spine J.*, vol. 17, pp. 355–360, 2008.

[3] H. Corriveau, R. Hebert, and F. Prince, "Postural control in the ederly: An analysis if test–retest and interrater reliability of the COP–COM variable," *Arch. Phys. Med. Rehabil.*, vol. 82, pp. 80–85, 2001.

[4] F. De la Huerta, M. A. Leroux, and K. F. Zabjek, "Stereovideographic evaluation of the postural geometry of healthy and scoliotic patients," *Ann. Chirurgie*, vol. 52, pp. 776–783, 1998.

[5] S. K. Banala, S. K. Agrawal, and A. Fattah, "A gravity balancing leg orthosis for robotic rehabilitation," in *Proc. IEEE ICRA Conf.*, Barcelona, Spain, 2004, pp. 2474–2479.

[6] J. J. Buchanan and F. B. Horak, "Emergence of postural patterns as a function of vision and translation frequency," *J. Neurophysiol.*, vol. 81, pp. 2325–2339, 1999.

[7] S. E. Halliday, D. A. Winter, and J. S. Frank, "The initiation of gait in young, elderly and Parkinson's disease subjects," *J. Gait Posture*, vol. 8, pp. 8–14, 1998.

[8] Y. Jian, D. A. Winter, and M. G. Ishac, "Trajectory of the body COG and COP during initiation and termination of gait," *J. Gait Posture*, vol. 1, pp. 9–22, 1993.

[9] D. Winter, *Biomechanics and Motor Control of Human Movement*, 3rd ed. New York: Wiley, 2005.

[10] T. Shimba, "An estimation of center of gravity from force platform data," *J. Biomech.*, vol. 17, pp. 53–60, 1984.

[11] D. King and V. Zatiorsky, "Extracting gravity line displacement from stabilographic recordings," *J. Gait Posture*, vol. 6, pp. 27–38, 1997.

[12] Y. Brenière, "Why we walk the way we do?" *J. Motor Behav.*, vol. 28, pp. 291–298, 1996.

[13] O. Caron, B. Faure, and Y. Brenière, "Estimating the center of gravity of the body on the basis of the center of pressure in standing posture," *J. Biomech.*, vol. 30, pp. 1169–1171, 1997.

[14] A. L. Betker, Z. Moussaviand, and T. Szturm, "Center of mass function approximation," in *Proc. 26th IEEE EMBS*, San Francisco, CA, 2004, pp. 687–690.

[15] A. L. Betker, Z. Moussaviand, and T. Szturm, "Application of feedward propagation neural network to center of mass estimation for use in clinical environment," in *Proc. IEEE EMBS Conf.*, Cancun, Mexico, 2003, pp. 2714–2717.

[16] S. Cotton, A. Murray, and P. Fraisse, "Estimation of the center of mass using static equivalent serial chain modeling," presented at the ASME IDETC/CIE Conf., San Diego, CA, 2009.

[17] B. Espiau and R. Boulic, "On the computation and control of the mass center of articulated chains," INRIA, Grenoble, France, Res. Rep. 3479, 1998.

[18] S. Cotton, A. Murray, and P. Fraisse, "Statically equivalent serial chain for modeling the center of mass of humanoid robots," in *Proc. IEEE-RAS Humanoids Conf.*, Daejeon, South Korea, 2008, pp. 138–144.

[19] Z. Vafa and S. Dubowsky, "The kinematics and dynamics of space manipulators: The virtual manipulator approach," *Int. J. Robot. Res.*, vol. 9, pp. 3–21, 1990.

[20] S. Dubowsky and E. Papadopoulos, "The kinematic, dynamics and control of free-flying and free-floating space robotic systems," *IEEE Trans. Robot. Autom.*, vol. 9, no. 5, pp. 531–543, Oct. 1993.

[21] S. Agrawal, G. Gardner, and S. Pledgie, "Design and fabrication of a gravity balanced planar mechanism using auxiliary parallelograms," *ASME J. Mech. Des.*, vol. 123, pp. 525–528, 2001.

Stabilizing and Direction Control of Efficient 3-D Biped Walking Based on PDAC

Tadayoshi Aoyama, Yasuhisa Hasegawa, Kosuke Sekiyama, and Toshio Fukuda

***Abstract*—This paper proposes a 3-D biped dynamic walking algorithm based on passive dynamic autonomous control (PDAC). The robot dynamics is modeled as an autonomous system of a 3-D inverted pendulum by applying the PDAC concept that is based on the assumption of point contact of the robot foot and the virtual constraint as to robot joints. Due to autonomy, there are two conservative quantities named "PDAC constant," which determine the velocity and direction of the biped walking. We also propose the convergence algorithm to make PDAC constants converge to arbitrary values, so that walking velocity and direction are controllable. Finally, experimental results validate the performance and the energy efficiency of the proposed algorithm.**

***Index Terms*—Biped walking, legged robots, underactuate.**

I. INTRODUCTION

By assuming a point contact between a robot foot and the ground and using a robot inherent dynamics, a natural and efficient bipedal walking has been realized. Grizzle and Westervelt *et al.* built the controller by the use of *virtual constraint* that realizes the stable dynamic walking by means of the planar biped robot with a torso [1]–[3]. Also, it is reported to propose analytical 3-D biped walking control method for a five-link bipedal robot based on the point contact [4], [5]. A few works realized 3-D biped walking with an experimental robot. Fukuda *et al.* realized 3-D dynamic walking with the experimental robot based on the assumption that the sagittal and lateral motions can be separated [6]. However, this control method has a problem in dividing 3-D dynamics when the dynamics of each plane is closely coupled. In order to solve this problem, we apply the passive dynamic autonomous control (PDAC) [7], which is one of the point contact methods, to a 3-D dynamics of the robot without dividing.

We model a biped robot as a 3-D inverted pendulum. By applying the PDAC, a 3-D dynamics is expressed as a 2-D autonomous system. This 2-D autonomous system has two conservative quantities named as "PDAC constant." Since two PDAC constants determine the walking velocity and the walking direction of the robot, the velocity and the direction of the walking are converged into the desired ones by controlling the two PDAC constants. This paper proposes the two controllers for two PDAC constants and confirms the convergence of two constants in numerical simulations. Finally, experimental results validate that the proposed algorithm realizes the stable and energy efficient walk.

Manuscript received March 1, 2009; revised June 29, 2009. First published October 20, 2009; current version published November 11, 2009. Recommended by Guest Editor J.-P. Laumond.

T. Aoyama, K. Sekiyama, and T. Fukuda are with the Department of Micro-Nano Systems Engineering, Nagoya University, Nagoya 464-8603, Japan (e-mail: aoyama@robo.mein.nagoya-u.ac.jp; sekiyama@mein.nagoya-u.ac.jp; fukuda@mein.nagoya-u.ac.jp).

Y. Hasegawa is with the Department of Intelligent Interaction Technologies, University of Tsukuba, Tsukuba 305-8573, Japan (e-mail: hase@esys.tsukuba.ac.jp).

Color versions of one or more of the figures in this paper are available online at http://ieeexplore.ieee.org.

Digital Object Identifier 10.1109/TMECH.2009.2032777

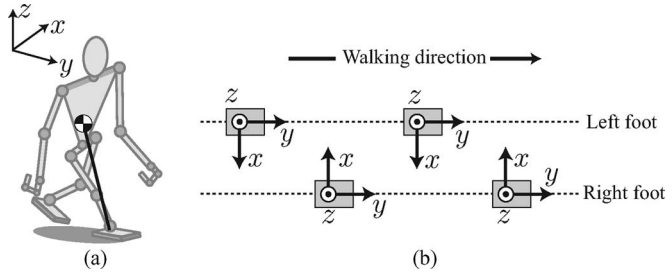

Fig. 1. (a) 3-D inverted pendulum model. (b) Definition of coordinate system. Note that this figure shows only a coordinate system definition and does not mean that foot placement is in alignment.

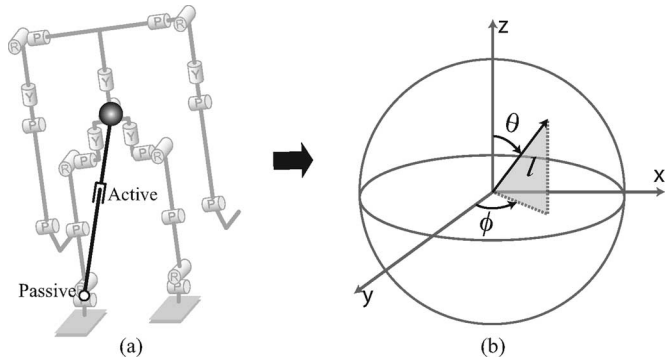

Fig. 2. (a) Passive joints (point contact) and active pendulum length actuation. (b) Polar coordinate system around contact point.

II. Model

A. 3-D Inverted Pendulum Model

In this paper, a robot is modeled as a 3-D inverted pendulum, as shown in Fig. 1(a). We utilize the polar coordinate system, and the state variables and parameters are shown in Fig. 2(b). By applying PDAC, dynamic equations of 3-D inverted pendulum are expressed as follows:

$$\frac{d}{dt}\left(ml^2 \sin^2\theta\dot{\phi}\right) = 0 \tag{1}$$

and

$$\frac{d}{dt}\left(ml^2\dot{\theta}\right) = ml^2\dot{\phi}^2 \sin\theta\cos\theta + mgl\sin\theta \tag{2}$$

where θ and ϕ are the variables of the pendulum angle around the contact point, and l is the variable of the pendulum length. The detailed calculation process of (1) and (2) is given in [8]. By multiplying both sides of (1) by $ml^2 \sin^2\theta\dot{\phi}$ and integrating with respect to time, the following constraint equation is obtained:

$$\dot{\phi} = \frac{\sqrt{2C_1}}{ml^2 \sin^2\theta} \tag{3}$$

$$:= F_1(\theta) \tag{4}$$

where C_1 is the integral constant. Substituting (3) into (2) results in

$$\dot{\theta} = \frac{1}{ml^2}\sqrt{2\int\left(\frac{2C_1\cos\theta}{\sin^3\theta} + m^2gl^3\sin\theta d\theta\right)} \tag{5}$$

$$:= \frac{1}{M(\theta)}\sqrt{2\big(D(\theta)+C_2\big)} \tag{6}$$

$$:= F_2(\theta) \tag{7}$$

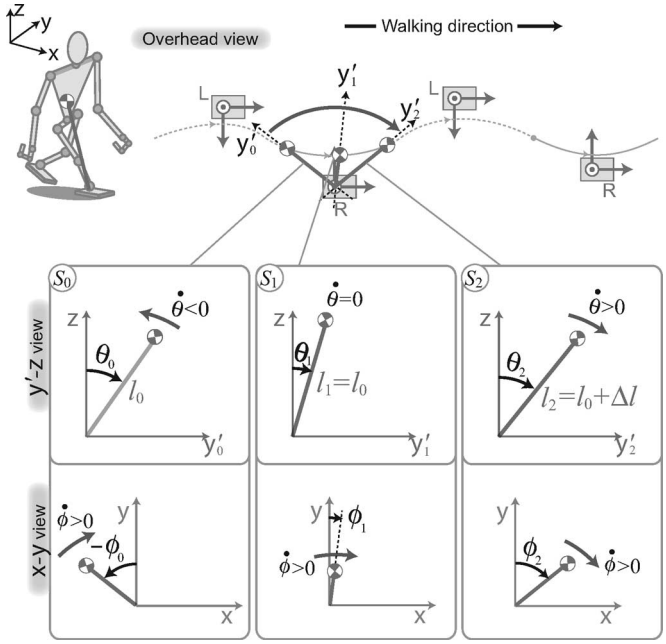

Fig. 3. Parameters and variables of dynamic walking based on 3-D inverted pendulum model.

where C_2 is the integral constant. We call C_1 and C_2 "PDAC constant," which are determined by initial state immediately after a foot contact. Next, in accordance to PDAC, the pendulum length is described as the function of θ as

$$l := \lambda(\theta). \tag{8}$$

In this paper, for simplicity, λ is defined as a function of θ as follows:

$$\lambda(\theta) =: \sqrt[3]{p_1\theta^3 + p_2\theta^2 + p_3\theta^+ p_4} \tag{9}$$

$$=: \sqrt[3]{f(\theta)}. \tag{10}$$

By substituting this equation into (6), the converged dynamics are derived as

$$M(\theta) = mf(\theta)^{2/3} \tag{11}$$

$$D(\theta) = -\frac{C_1}{\sin^2\theta} - m^2g\big((f(\theta) - f''(\theta)\big)\cos\theta - (f'(\theta) - f'''(\theta))\sin\theta). \tag{12}$$

B. Design of Walking Cycle

In this section, the actual motion of the robot is designed. Fig. 3 shows the parameters and variables of the pendulum motion. S_0 and S_2 denote moments right before and after a foot contact, and S_1 is a moment at $\dot{\theta} = 0$. The variables θ_i, ϕ_i, and l_i denote the roll angle, yaw angle, and pendulum length at S_i $(i = 0, 1, 2)$, respectively. During a cycle of walking motion, ϕ is monotonically increasing. Meanwhile, θ decreases at first, and then increases, after posing for a moment at θ_1. Thus, we compartmentalize a walking cycle from a foot contact to the next foot contact into two phases—phase (A): from S_0 to S_1 $(\dot{\theta} < 0)$; phase (B): from S_1 to S_2 $(\dot{\theta} > 0)$. In phase (A), the pendulum length is constant; thus, the coefficients p_1–p_4 in (9) are

$$p_1 = p_2 = p_3 = 0 \tag{13}$$

$$p_d = l_0^3. \tag{14}$$

In phase (B), the coefficients p_1–p_4 are decided so that the following four conditions are satisfied:

$$f(\theta_1) = l_1^3 \tag{15}$$

$$f(\theta_2) = l_2^3 \tag{16}$$

$$f'(\theta_2) = 0 \tag{17}$$

and

$$-f''(\theta_1)\cos\theta_1 + \big(-f'(\theta_1) + f'''(\theta_1)\big)\sin\theta_1 = 0. \tag{18}$$

Equations (15) and (16) signify the condition of pendulum length continuity, and (17) is the condition that the velocity of the pendulum along l is 0 at a foot contact. The objective of (18) is to match PDAC constants of the phases (A) and (B).

From (15)–(18), the coefficients p_1–p_4 are derived as follows:

$$p_1 = -\frac{l_2^3 - l_0^3}{(\theta_2 - \theta_1)^2}\frac{u_3}{u_1 u_3 - u_2} \tag{19}$$

$$p_2 = -\frac{l_2^3 - l_0^3}{(\theta_2 - \theta_1)^2}\frac{u_2}{u_1 u_3 - u_2} \tag{20}$$

$$p_3 = -3p_1\theta_2^2 - 2p_2\theta_2 \tag{21}$$

and

$$p_4 = l_2^3 - p_1\theta_2^3 - p_2\theta_2^2 - p_3\theta_2 \tag{22}$$

where

$$u_1 = 2\theta_2 + \theta_1 \tag{23}$$

$$u_2 = -6\theta_1\cos\theta_1 - 3\theta_1^2\sin\theta_1 + 6\sin\theta_1 + 3\theta_2^2\sin\theta_1 \tag{24}$$

and

$$u_3 = -2\cos\theta_1 - 2\theta_1\sin\theta_1 + 2\theta_2\sin\theta_1. \tag{25}$$

C. Foot Contact Model

In this paper, it is assumed that perfectly inelastic collision between the ground and a foot occurrs for a moment, similarly to previous works [1], [3], [5]. Thus, the angular momentum around a new contact point is conserved. Assuming that ϕ_0 is the angle of ϕ right after a foot contact, a vector of the pendulum after impact, $\boldsymbol{L}$, is

$$\boldsymbol{L} = [l_0\sin\phi_0\sin\theta_0, l_0\cos\phi_0\sin\theta_0, l_0\cos\theta_0]^T \tag{26}$$

where ϕ_0 and θ_0 are angles in the coordinate system of the next step.

The velocity vector right before a foot contact, $\boldsymbol{V}_1$, is calculated as follows:

$$\boldsymbol{V}_1 = [v_x, v_y, v_z]^T \tag{27}$$

where

$$\begin{aligned} v_x &= l_2(\dot\phi_2\cos\phi_2\sin\theta_2 + \dot\theta_2\sin\phi_2\cos\theta_2) \\ &\quad + \dot l_2(\sin\phi_2\sin\theta_2) \\ v_y &= l_2(-\dot\phi_2\sin\phi_2\sin\theta_2 + \dot\theta_2\cos\phi_2\cos\theta_2) \\ &\quad + \dot l_2(\cos\phi_2\sin\theta_2) \end{aligned}$$

and

$$v_z = -l_2\dot\theta_2\sin\theta_2 + \dot l_2(\cos\theta_2)$$

with ϕ_2 being the angle of ϕ before the foot contact.

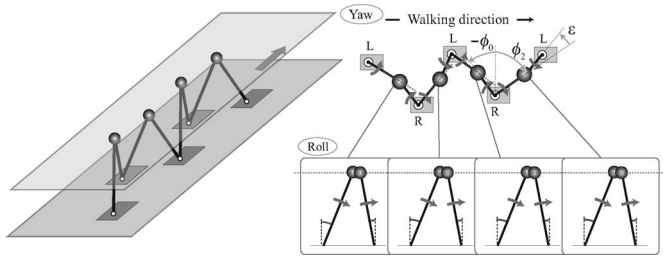

Fig. 4. Geometrical constraints at foot contact.

The velocity vector after a foot contact, $\boldsymbol{V}_0$, is derived by the following equation:

$$\boldsymbol{V_0} = \frac{\boldsymbol{V_1}(\boldsymbol{L}\times(\boldsymbol{V_1}\times\boldsymbol{L}))}{|\boldsymbol{L}\times(\boldsymbol{V_1}\times\boldsymbol{L})|}(\boldsymbol{L}\times(\boldsymbol{V_1}\times\boldsymbol{L})) \tag{28}$$

$$= \frac{\boldsymbol{L}\times(\boldsymbol{V_1}\times\boldsymbol{L})}{l^2} \tag{29}$$

$$:= [v_x', v_y', v_z']^T. \tag{30}$$

Note that $\boldsymbol{V_1}$ is $[-v_x, v_y, v_z]^T$ since left- and right-handed systems are switched at a foot contact.

From (30), $\dot\theta_0$ and $\dot\phi_0$ are

$$\dot\theta_0 = -\frac{v_z'}{l_0\sin\theta_0} \tag{31}$$

and

$$\dot\phi_0 = -\frac{\sin\phi_0\cos\theta_0}{\cos\phi_0\sin\theta_0}\dot\theta_0 - \frac{v_x'}{l_0\cos\phi_0\sin\theta_0}. \tag{32}$$

III. Stabilization

A. Geometrical Constraints

In order to stabilize walking, some geometrical constraints are given. At first, a displacement of a pendulum length is fixed to a constant value. In this constraint, a supplied energy is almost constant. In addition, the following two constraints about a foot contact are designed, as shown in Fig. 4.

1) The height of center of gravity (COG) h at a foot contact is constant, i.e., roll angles of stance and swing leg are constant at a foot contact.
2) Yaw angle of a swing leg is shifted by ϵ from the symmetrical position with a stance leg at a foot contact, i.e., it is $\phi_0[k+1] = -\phi_2[k] + \epsilon$, where $\phi_0[k+1]$ and $\phi_2[k]$ denote ϕ_0 and ϕ_2 at the $(k+1)$th and kth steps, respectively.

B. Stabilization Based on PDAC Constant

In this section, we propose the novel stabilizing control by the use of PDAC constants. The 2-D converged dynamics has two conserved quantities, i.e., PDAC constants C_1 and C_2, as can be seen in (4) and (7). These two PDAC constants determine the trajectory in the 3-D space composed of θ, $\dot\theta$, and $\dot\phi$, i.e., the robot dynamics. Note that ϕ, which decides only the direction of the pendulum, is directly independent of θ, $\dot\theta$, and $\dot\phi$ [see (4) and (7)]. Thus, in order to build the controller that stabilizes bipedal walking in the 4-D space composed of θ, ϕ, $\dot\theta$, and $\dot\phi$, it is necessary to design the following two controllers: 1) the convergent controller of PDAC constant for stabilizing the dynamics and 2) the walking direction controller for deciding the walking direction of the robot. Hereinafter, controller 1) is described first, and then

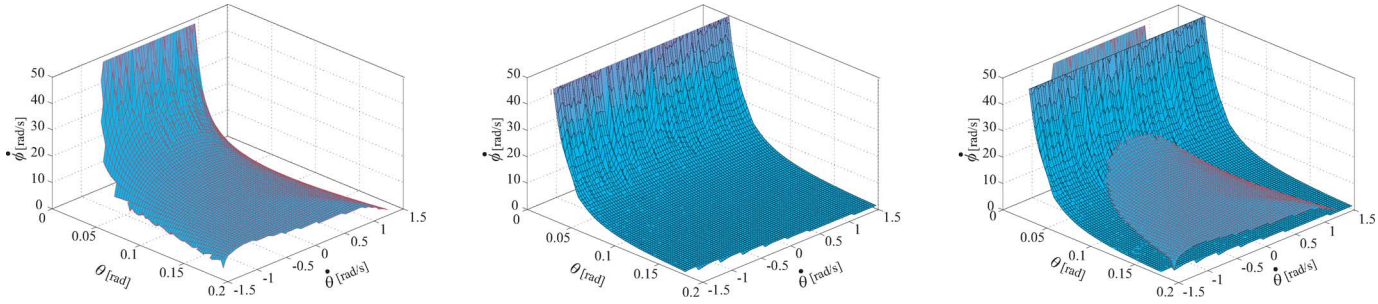

Fig. 5. (Left) Manifolds of 3-D space composed of θ, $\dot{\theta}$, and $\dot{\phi}$. (Middle) Constant C_2 manifold ($C_2 = 456$). (Right) Constant C_1 manifold ($C_1 = 0.02$).

2) is explained. We show the process of convergence and stabilization by means of return maps.

1) Convergent Controller of PDAC Constants: Two PDAC constants that determine the robot dynamics keep certain values respectively until a next foot contact. Values of the two PDAC constants are derived from the condition immediately after a foot contact; also, two PDAC constants are redetermined at every foot contact, respectively. Therefore, stabilization can be realized if two PDAC constants converge to the desired values at every step. In order to converge PDAC constants to the desired values, it is necessary to find the condition of l_2, h, and ϵ. Hence, the constraint condition satisfying the desired PDAC constants is derived.

At first, convergent values of PDAC constants are obtained. Letting PDAC constants at the kth step to be $C_1[k]$ and $C_2[k]$, $C_1[k+1]$ and $C_2[k+1]$ are described as follows from (4), (7), (31) and (32):

$$C_1[k+1] = \left(R_{11}\sqrt{C_1[k]} + R_{12}\sqrt{A}\right)^2 \tag{33}$$

$$=: \xi_1(C_1[k], C_2[k], \theta_0, \theta_2, \epsilon, l_2) \tag{34}$$

$$C_2[k+1] = \left(R_{21}\sqrt{C_1[k]} + R_{22}\sqrt{A}\right)^2 + \frac{1}{\sin^2\theta_0}\left(R_{11}\sqrt{C_1[k]} + R_{12}\sqrt{A}\right)^2 + m^2 g l_0^3 \cos\theta_0 \tag{35}$$

$$=: \xi_2(C_1[k], C_2[k], \theta_0, \theta_2, \epsilon, l_2) \tag{36}$$

where

$$R_{11} = \frac{l_0 \sin\theta_0 \cos\epsilon}{l_2 \sin\theta_2} \tag{37}$$

$$R_{12} = \frac{l_0 \sin\theta_0 \cos\theta_2 \sin\epsilon}{l_2} \tag{38}$$

$$R_{21} = \frac{l_0 \cos\theta_0 \sin\epsilon}{l_2 \sin\theta_2} \tag{39}$$

$$R_{22} = \frac{l_0}{l_2}\left(\sin\theta_0\theta_2 - \cos\theta_0 \cos\theta_2 \cos\epsilon\right) \tag{40}$$

and

$$A = \frac{-C_1[k]}{\sin^2\theta_2} + D(\theta_2) + C_2[k]. \tag{41}$$

Note that l_0 is a constant value.

Assuming that $C_1[k] = C_1[k+1] = C_1^*$ and $C_2[k] = C_2[k+1] = C_2^*$, (34) and (36) at stable points are described as follows:

$$C_1^* = \left(R_{11}\sqrt{C_1^*} + R_{12}\sqrt{B}\right)^2 \tag{42}$$

$$=: \xi_1(C_1^*, C_2^*, \theta_0, \theta_2, \epsilon, l_2) \tag{43}$$

$$C_2^* = \left(R_{21}\sqrt{C_1[k]} + R_{22}\sqrt{B}\right)^2 + \frac{1}{\sin^2\theta_0}\left(R_{11}\sqrt{C_1[k]} + R_{12}\sqrt{B}\right)^2 + m^2 g l_0^3 \cos\theta_0 \tag{44}$$

$$=: \xi_2(C_1^*, C_2^*, \theta_0, \theta_2, \epsilon, l_2) \tag{45}$$

where

$$B = \frac{-C_1^*}{\sin^2\theta_2} + D(\theta_2) + C_2^*. \tag{46}$$

Thus, the convergent PDAC constants C_1^* and C_2^* are derived as follows:

$$C_1^* = -\frac{m^2 g l_0^3 \cos\theta_0 + D(\theta_2)}{\left(R_{21} + R_{22}\sqrt{1/(\sin^2\theta_0) - 1/(\sin^2\theta_2) + (1-R_{11})^2/R_{12}^2}\right)^2} + \frac{(1-R_{11})^2}{R_{12}^2} \tag{47}$$

$$=: \eta_1(\theta_0, \theta_2, \epsilon, l_2) \tag{48}$$

$$C_2^* = D(\theta_2) - \left(\frac{1}{\sin^2\theta_0} + \frac{(1-R_{11})^2}{R_{12}^2}\right) C_1^* \tag{49}$$

$$=: \eta_2(\theta_0, \theta_2, \epsilon, l_2). \tag{50}$$

The geometrical constraint h represents the relationship of θ_0, θ_2, and l_2, i.e.,

$$h = l_0 \cos\theta_0 \tag{51}$$

$$= l_2 \cos\theta_2. \tag{52}$$

Hence, from (48), and (50)–(52), it is possible to decide θ_0, θ_2, ϵ, and l_2 by Newton–Raphson method.

By employing θ_0, θ_2, ϵ, and l_2 satisfying (48) and (50), if $C_1[k] = C_1^*$ and $C_2[k] = C_2^*$, then $C_1[k+1] = C_1^*$ and $C_2[k+1] = C_2^*$. Thus, if C_1^* and C_2^* exist and are unique, and if $|\frac{\partial \xi_1}{\partial C_1}| < 1$ and $|\frac{\partial \xi_2}{\partial C_2}| < 1$ in the vicinity of (C_1^*, C_2^*), PDAC constants are converged on a fixed point. Fig. 5 shows the constant C_2 manifold and the constant C_1 manifold in a 3-D space composed of θ, $\dot{\theta}$, and $\dot{\phi}$. If C_2 is converged on $C_2^* = 456$, the trajectory in the 3-D space composed of $(\theta, \dot{\theta}, \dot{\phi})$ is attracted to the manifold depicted in Fig. 5 (left). Similarly, if C_1 has converged on 0.02, the trajectory is attracted to the manifold shown in Fig. 5 (middle). Consequently, if C_1 and C_2 are converged on (C_1^*, C_2^*), the robot state is attracted to the trajectory composed of both manifolds, as shown in Fig. 5 (right). Fig. 6 (top and bottom) shows, respectively, the return maps of C_1 and C_2 under the condition of $(C_1^*, C_2^*) = (0.02, 456.0)$. As can be seen in this figure, C_1 and C_2

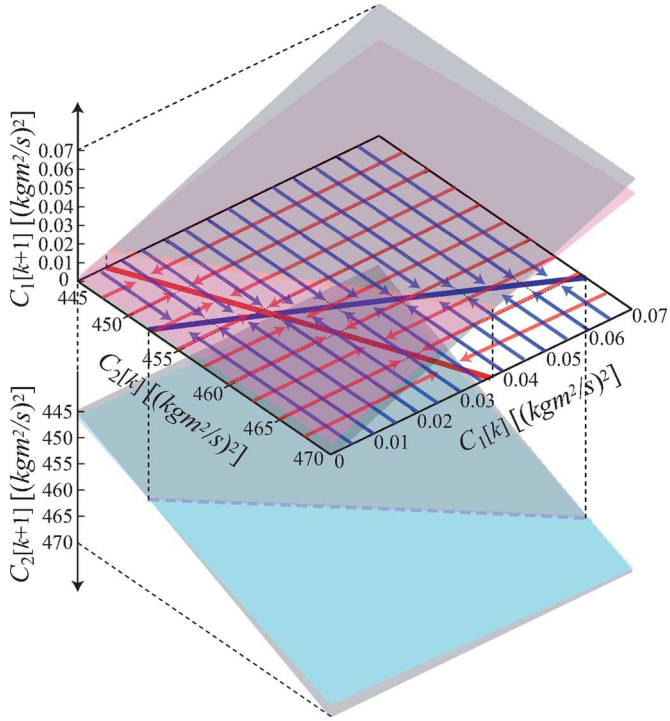

Fig. 6. Return map of C_1 and C_2 ($C_1^* = 0.02$, $C_2^* = 456.0$, $h = 0.428$, and $l_0 = 0.455$).

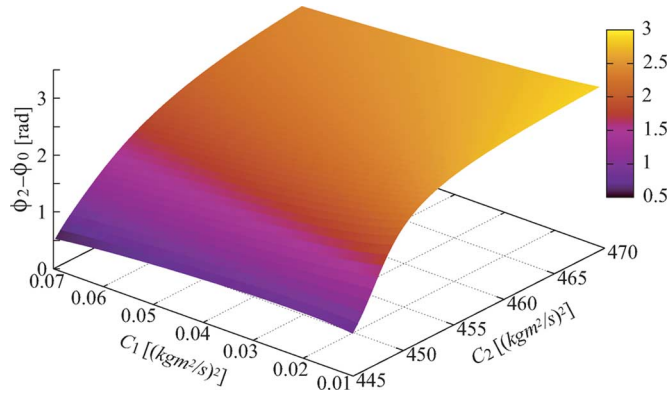

Fig. 7. 3-D map of C_1^*, C_2^*, and $\phi_2 - \phi_0$.

possess the stable fixed points at C_1^* and C_2^*. Therefore, C_1 and C_2 converge to C_1^* and C_2^*, respectively. That is, the trajectory in the 3-D space composed of θ, $\dot{\theta}$, and $\dot{\phi}$ converge to a sole trajectory determined by C_1^*, C_2^*, and h.

2) Walking Direction Controller: Next, we design the walking direction controller. Since ϕ is independent of the robot dynamics, ϕ determines only a walking direction. Thus, the walking direction is determined by the phase portrait of ϕ. If two-cycle trajectory occurs in the phase space of ϕ, the robot walks to the right or left direction. That is to say, by adjusting the degree of the error from one-cycle trajectory, i.e., the degree of two cycles, it is possible to control the walking direction. The difference of two cycles in the phase space of ϕ should be controlled arbitrary in order to walk in the desired direction.

Fig. 7 shows the relationship between PDAC constants, C_1^*, C_2^*, and the variation of ϕ for a step, $\phi_2 - \phi_0$. As can be seen in this figure, the variation of ϕ monotonically increases with respect to C_2^* and monotonically decreases with respect to C_1^*. Besides, it can be

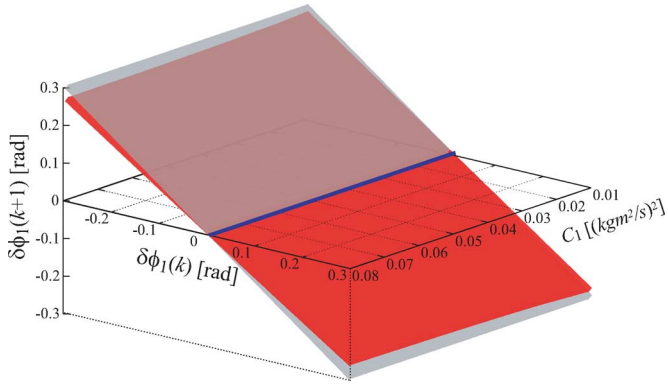

Fig. 8. Return map of $\delta\phi_1$ with respect to C_1^* ($C_2^* = 456.0$, $g_\phi = 0.3$, $h = 0.428$, and $l_0 = 0.455$).

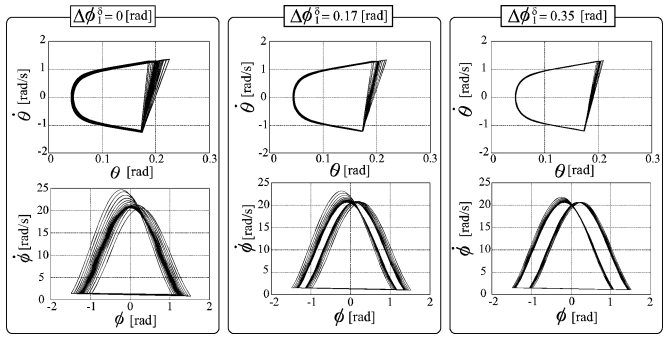

Fig. 9. Phase portrait of θ and ϕ ($C_1^* = 0.02$, $C_2^* = 456.0$, $h = 0.428$, $l_0 = 0.455$, $g_\phi = 0.3$, and $\sigma = 1$). (Left) $\phi_1^d = 0$ (in radians). (Middle) $\phi_1^d = 0.17$ (in radians) (Right) $\phi_1^d = 0.35$ (in radians).

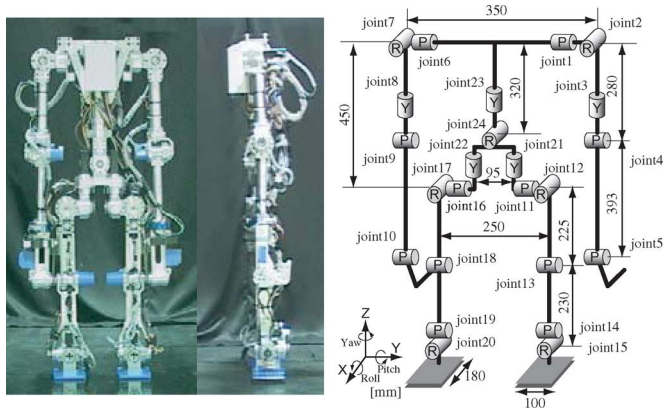

Fig. 10. Gorilla robot Ⅲ (multilocomotion robot) [9]. This robot is multilocomotive; it can perform biped locomotion, quadruped locomotion, and brachiation.

seen from this figure that the effect of C_2^* on the variation of ϕ is large, whereas that of C_1^* is quite small. Thus, to adjust the two cycles of the trajectory in the phase space of ϕ, C_1^* and C_2^* are determined according to the following equations:

$$C_1^* = C_1^d \tag{53}$$

$$C_2^* = C_2^d + g_\phi \left(\phi_1[k] - \phi_1[k+1] + (-1)^k \sigma \phi_1^d\right) \tag{54}$$

where

$$\sigma = \begin{cases} 1, & \text{left direction} \\ -1, & \text{right direction} \end{cases} \tag{55}$$

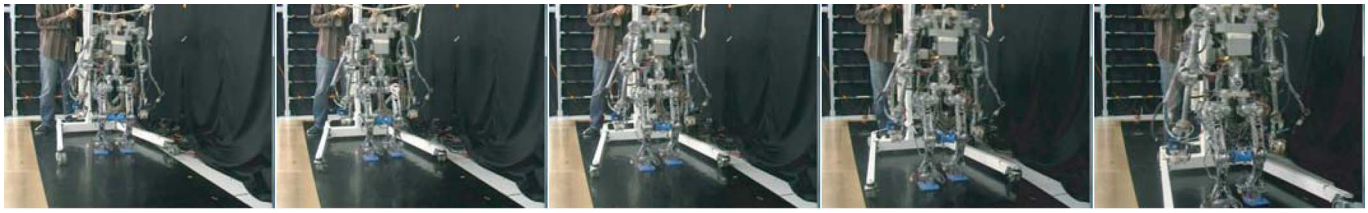

Fig. 11. Snapshots of the bipedal walking experiment. Each figure shows the snapshots at the (a) 1st, (b) 7th, (c) 13th, (d) 19th, and (e) 25th steps.

C_1^* and C_2^* are the desired PDAC constants, g_ϕ is the feedback gain of the direction, $\phi_1[k]$ and $\phi_1[k-1]$ are ϕ_1 values at present and previous steps, and ϕ_1^d is the desired angle, which is determined by the desired walking direction, e.g., $\phi_1^d = 0$ if the desired walking direction is straight. Note that ϕ_1 is the yaw angle at $\dot{\theta} = 0$ (see Fig. 3).

Fig. 8 shows the return map of $\delta\phi[k]$ with respect to C_1^* under the condition of $g_\phi = 0.3$ and $C_2^* = 456.0$. From this figure, it can be seen that $\delta\phi$ possesses the stable fixed point at 0. Hence, the walking direction can be controlled stably by (53) and (54).

Fig. 9 depicts the phase portrait of θ and ϕ under the condition that $C_1^* = 0.02$, $C_2^* = 456.0$, $h = 0.428$, $l_0 = 0.455$, $g_\phi = 0.3$, and $\sigma = 1$. As can be seen from these portraits, the proposed walk direction control achieves the desired two-cycle trajectory of the phase space of ϕ. In a practical use, the robot updates ϕ_1^d regularly according to the information of a target direction given by a controller or a user. As a result, it is conceivable that the robot gets close to the target gradually, and reach the desired direction finally. The convergence of the trajectory is confirmed by the phase portrait of θ in Fig. 9. Thus, the trajectory in the 3-D space composed of θ, $\dot{\theta}$, and $\dot{\phi}$ also converges to a sole trajectory.

IV. Experiment

A. Experimental Setup

Fig. 10 depicts the overview of our robot "Gorilla Robot Ⅲ (Multi-Locomotion Robot)" [9] and its link structure. The robot is about 1.0 m tall, weighs about 24.0 kg, and consists of 25 links and 24 motors including two grippers. The real-time operating system VxWorks (wind river systems) runs on a Pentium Ⅲ PC for processing sensory data and generating its behaviors. Each joint is driven by an ac servo motor through the harmonic drive gear, partially through a timing belt. Maximum output power of the motor is 30 W. The power supply and the computer are installed outside of the robot for weight saving.

B. Experimental Result

We validated the proposed algorithm with the Gorilla Robot Ⅲ. The experiment was conducted on the level ground with maximum $\pm$1.0 cm irregularity under the condition that the desired direction is straight ($\phi_1^d = 0$). As a result of the experiment, 3-D dynamic walking in 0.14 m step length and 0.26 m/s walking velocity was realized. Although the ground has maximum $\pm$1.0 cm irregularity in the experimental environment and the information of the ground shape was not given to the robot, the robot achieved the stable walking. Fig. 11. shows snapshots of the experiment. Also, Figs. 12 and 13 show the joint angles and joint torques of the experiment, respectively. It is confirmed from Fig. 12 that the cyclic trajectories change to large ones gradually.

C. Energy Efficiency

The biped walk of the Gorilla Robot Ⅲ is also evaluated based on the dimensionless specific mechanical cost of transport, $C_{\mathrm{mt}} =$

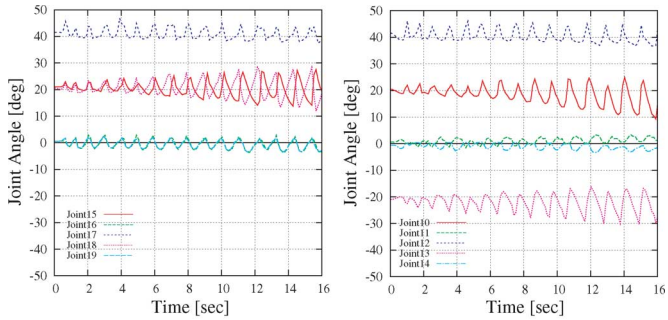

Fig. 12. Joint angle of the bipedal walking experiment. (a) Joint angles of the left leg. (b) Joint angles of the right leg.

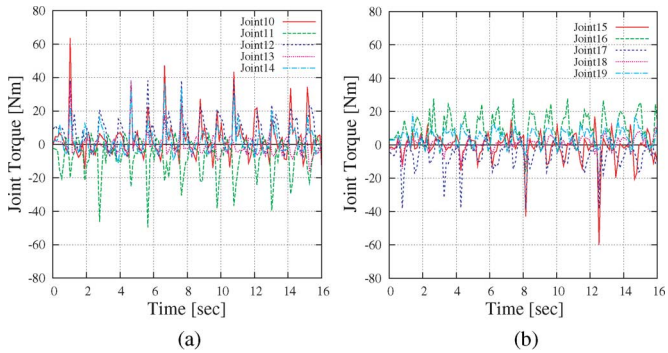

Fig. 13. Torque output of the bipedal walking experiment. (a) Joint torque of the left leg. (b) Joint torque of the right leg.

(consumed mechanical energy)/(weight$\times$distance traveled) [10]. The C_{mt} affords to compare energy efficiency between robots with different sizes and weights. The mechanical work in one cycle of a walking, E, is calculated as follows:

$$E = \int_0^T \sum_{i=1}^{N} \delta\left(\tau_i \dot{\theta}_i\right) dt$$

$$\text{where } \delta(x) = \begin{cases} x, & \text{if } x > 0 \\ 0, & \text{if } x \leq 0 \end{cases} \tag{56}$$

T is the cycle time of a walk, N is the number of actuators, and τ_i and $\dot{\theta}_i$ are the joint torque and the angular velocity of the ith joint number. After convergence of the motion, the C_{mt} of the robot is 0.15, while the C_{mt} of Honda humanoid ASIMO [11], which realized a stable 3-D dynamic walking by appling zero moment point (ZMP) based control, is estimated to be about 1.6 in [10]. The efficiency of our walk is therefore more than ten times as high as one of the ZMP-based walk. In addition to this consideration, we conducted the experiment of linear inverted pendulum model (LIPM) based walking [12] as another

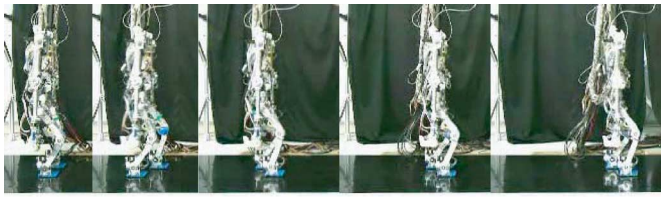

Fig. 14. Snapshots of the LIPM-based bipedal walking experiment. Each figure shows the snapshots at the (a) 1st, (b) 2nd, (c) 3rd, (d) 4th, and (e) 6th steps.

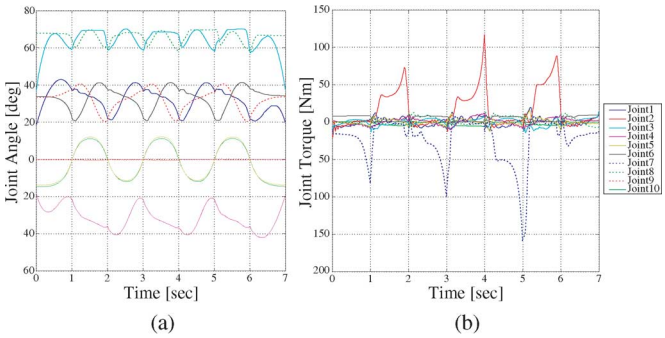

Fig. 15. Joint angle and torque output of the bipedal walking experiment.

TABLE I
COMPARISON OF THE C_{mt}

Method (Hardware)	C_{mt}
PDAC-based method (Gorilla Robot)	0.15
LIPM-based method (Gorilla Robot)	0.57
ZMP-based method (ASIMO)	1.6 (from [10])

example of the comparing method. Figs. 14 and 15 show the snapshots and data of the experiment, respectively. From the experimental data, C_{mt} of the LIPM-based walking is estimated to be about 0.57. Table I shows C_{mt} of each method. These results validate the efficiency of the proposed method.

V. CONCLUSION

This paper proposed the 3-D biped dynamic walking algorithm based on the PDAC. The robot dynamics are modeled as an autonomous system of a 3-D inverted pendulum by applying the PDAC. We numerically presented that two conservative quantities named PDAC constant determine the velocity and the walking direction of the biped walk. We also proposed the two controllers for two PDAC constants and confirmed a convergence of the two constants in numerical simulations. Finally, experimental results validated the performance and the energy efficiency of the proposed algorithm.

REFERENCES

[1] J. W. Grizzle, G. Abba, and F. Plestan, "Asymptotically stable walking for biped robots: Analysis via systems with impulse effects," *IEEE Trans. Autom. Control*, vol. 46, no. 1, pp. 51–64, Jan. 2001.
[2] E. R. Westervelt, J. W. Grizzle, and D. E. Koditschek, "Hybrid zero dynamics of planar biped walkers," *IEEE Trans. Autom. Control*, vol. 48, no. 1, pp. 42–56, Jan. 2003.
[3] E. R. Westervelt, G. Buche, and J. Grizzle, "Experimental validation of a framework for the design of controllers that induce stable walking in planar bipeds," *Int. J. Robot. Res.*, vol. 23, no. 6, pp. 559–582, 2004.
[4] G. Song and M. Zefran, "Underactuated dynamic three-dimensional bipedal walking," in *Proc. IEEE Int. Conf. Robot. Autom.*, 2006, pp. 854–859.
[5] C. Chevallereau, J. W. Grizzle, and C.-L. Shih, "Asymptotically stable walking of a five-link underactuated 3-D bipedal robot," *IEEE Trans. Robot.*, vol. 25, no. 1, pp. 37–50, Feb. 2009.
[6] T. Fukuda, M. Doi, Y. Hasegawa, and H. Kajima, "Multi-locomotion control of biped locomotion brachiation robot," in *Fast Motions in Biomechanics and Robotics: Optimization and Feedback Control*, Berlin, Germany: Springer-Verlag, 2006, pp. 121–145.
[7] M. Doi, Y. Hasegawa, and T. Fukuda, "Passive dynamic autonomous control of bipedal walking," in *Proc. IEEE/RAS Int. Conf. Hum. Robots*, 2004, pp. 811–829.
[8] M. Doi, Y. Hasegawa, and T. Fukuda, "3D dynamic walking based on the inverted pendulum model with two degree of underactuation," in *Proc. IEEE/RSJ Int. Conf. Intell. Robots Syst.*, 2005, pp. 2788–2793.
[9] H. Kajima, M. Doi, Y. Hasegawa, and T. Fukuda, "Study on brachiation controller for the multi-locomotion robot -redesigning behavior controllers," in *Proc. IEEE/RSJ Int. Conf. Intell. Robots Syst.*, 2003, pp. 1388–1393.
[10] S. Collins, A. Ruina, R. Tedrake, and M. Wisse, "Efficient bipedal robots based on passive-dynamic walkers," *Science*, vol. 307, pp. 1082–1085, 2005.
[11] Y. Sakagami, R. Watanabe, C. Aoyama, S. Matsunaga, N. Higaki, and K. Fujimura, "The intelligent ASIMO: System overview and integration," in *Proc. IEEE/RSJ Int. Conf. Intell. Robots Syst.*, 2002, pp. 2478–2483.
[12] S. Kajita, F. Kanehiro, K. Kaneko, K. Fujiwara, K. Yokoi, and H. Hirukawa, "Biped walking pattern generation by a simple three-dimensional inverted pendulum model," *Adv. Robot.*, vol. 17, no. 2, pp. 131–147, 2003.

Grip Control Using Biomimetic Tactile Sensing Systems

Nicholas Wettels, Avinash R. Parnandi, Ji-Hyun Moon, Gerald E. Loeb, and Gaurav S. Sukhatme

***Abstract*—We present a proof-of-concept for controlling the grasp of an anthropomorphic mechatronic prosthetic hand by using a biomimetic tactile sensor, Bayesian inference, and simple algorithms for estimation and control. The sensor takes advantage of its compliant mechanics to provide a triaxial force sensing end-effector for grasp control. By calculating normal and shear forces at the fingertip, the prosthetic hand is able to maintain perturbed objects within the force cone to prevent slip. A Kalman filter is used as a noise-robust method to calculate tangential forces. Biologically inspired algorithms and heuristics are presented that can be implemented online to support rapid, reflexive adjustments of grip.**

***Index Terms*—Biomimetic, dexterous manipulators, grip control, tactile sensor.**

Manuscript received February 25, 2009; revised June 26, 2009 and August 31, 2009. First published October 20, 2009; current version published November 11, 2009. Recommended by Guest Editor V. N. Krovi.

N. Wettels and G. E. Loeb are with the Department of Biomedical Engineering, University of Southern California, Los Angeles, CA 90089 USA (e-mail: nick.wettels@gmail.com; gloeb@usc.edu).
A. R. Parnandi is with the Department of Electrical Engineering, University of Southern California, Los Angeles, CA 90089 USA (e-mail: parnandi@usc.edu).
J.-H. Moon and G. S. Sukhatme are with the Department of Computer Science, University of Southern California, Los Angeles, CA 90089 USA (e-mail: jihyunmo@usc.edu; gaurav@usc.edu).

Color versions of one or more of the figures in this paper are available online at http://ieeexplore.ieee.org.
Digital Object Identifier 10.1109/TMECH.2009.2032686